Journal of Molecular Modeling (2019) 25: 84
https://doi.org/10.1007/s00894-019-3968-9

ORIGINAL PAPER

Motion in a crowded environment: the influence of obstacles' size and shape and model of transport

Piotr Polanowski[1] · Andrzej Sikorski[2]

Received: 21 November 2018 / Accepted: 8 February 2019 / Published online: 2 March 2019

Abstract

Simulations of motion in a complex crowded environment were performed. We employed the dynamic lattice liquid model, which was based on the cooperative movement concept. This algorithm is capable of working at very high densities, and the motion of all objects was highly correlated. The so-called motion of a single agent, where the motion of molecules is considered as a random walk without any correlation with other moving objects, was also calculated as the state of reference. Immobilized chains embedded in a two-dimensional triangular lattice modeled the crowded environment. The dynamic behavior of movable objects was studied and the influence of the structure of the matrix of obstacles on the molecular transport was discussed. It was shown that the type of transport has an impact on the dynamics of the system. The appearance and properties of subdiffusive motion were analyzed and referred to the structure of polymer systems.

Keywords Anomalous diffusion · Lattice model · Macromolecular crowding · Monte Carlo method

Introduction

Real biological environments are densely crowded with different components like lipids or proteins [1–6]. Transport phenomena play a crucial role in such inhomogeneous systems [1] but their dynamics are still far from being understood: experiments indicate a diversity of dynamic behavior the origin of which is being widely discussed [7–13]. These systems are mostly heterogeneous because the motion of molecules is hindered not only by fixed obstacles but also by numerous mobile objects, which can also be found there. The dynamics of biological crowded systems was experimentally studied using fluorescence correlation spectroscopy [1, 14–16], pulsed field gradient NMR [17], and single particle tracking SPT [6, 7, 18–23]. In some conditions an anomalous diffusion (a subdiffusive behavior) was mostly detected showing that the mean square displacement of objects $\langle \Delta r^2 \rangle$ scaled with time t as $\langle \Delta r^2 \rangle \sim t^{\alpha}$, with $\alpha < 1$ [6, 24–26]. SPT experiments gave values of this exponent between 0.2 and 0.9 [27].

Computer simulations of crowded environments also result in a subdiffusive motion of objects [27–31]. Usually, the presence of a matrix of fixed impenetrable obstacles results in an anomalous diffusion [8, 24], and thus the crowded environment in such a case can be modeled as a cluster of obstacles and the problem can be discussed using the theory of percolation. If the concentration of obstacles is lower than the percolation threshold, the diffusion is anomalous for a short time only. If the concentration of obstacles reaches the percolation threshold, the diffusion becomes anomalous over the whole time range [24, 32]. In the matrix of immobile obstacles at the percolation threshold, the exponent α is shown to be very close to 0.697 [14, 32–34]. In real biological systems, the presence of obstacles can also affect chemical reaction kinetics [35]. Simulations of such dense systems were performed using molecular dynamics and Brownian dynamics techniques employing both coarse-grained and atomistic models [35–49]. The results of initial Monte Carlo simulations of dense systems where cooperative motions were taken under consideration were recently published [50–52].

At high densities, the motion of a given object is correlated with the movement of neighboring objects. In this paper, we investigated the motion of objects in matrices of obstacles

This paper belongs to Topical Collection 8th conference on Modeling & Design of Molecular Materials (MDMM 2018)

✉ Andrzej Sikorski
sikorski@chem.uw.edu.pl

[1] Department of Molecular Physics, Technical University of Łódź, 90-924 Łódź, Poland

[2] Department of Chemistry, University of Warsaw, Pasteura 1, 02-093 Warsaw, Poland

having different sizes and shapes (protein or polymer chains) using two different models of transport. The first one was a single agent model (SAM), where the motion of each object takes place without any correlation with other moving objects. This model was also simulated to serve as a state of reference. The dynamic lattice liquid (DLL) model was used for these studies to study fully filled systems consisting of objects and obstacles without any vacancies. DLL can simulate dense systems using cooperative motion, and thus correlations of movement of objects were taken into consideration. Several works show the usefulness of this model in the study of complex macromolecular systems and crowded environments [53–60]. The comparison of results obtained for the models and their applicability were also discussed. The model system was two-dimensional and can be treated as a crude model of a cellular membrane [5, 48]. The excluded volume was the only potential used, and thus the system under consideration was athermal.

The present study enables us to include the cooperative motion of objects and to study the hydrodynamic properties of the system, which is crucial for diffusion in a crowded environment [46–48]. Thus, there is an important difference between the proposed treatment and other lattice models where motion was usually based on the concept of "an ant in the labyrinth", where the correlations of motion and also hydrodynamic effects are practically neglected [26, 61]. In the present work, strictly two-dimensional systems were studied and immobilized chains served as obstacles for movable solvent molecules. The relationship between the structure of polymer films and the motion of solvent was the study intent.

The structure of the paper is the following: in the next section "The models and the simulation methods" the basis of the DLL model are briefly described. The section "Results and discussion" presents the dynamics of objects in model systems with the emphasis on the anomalous diffusion and the comparison motion for all models under consideration. The last section "Conclusions" summarizes the main outcomes of the simulations.

The models and the simulation methods

The application of the DLL model and simulation method in the case of a crowded environment was described in detail in [53], and only a short description is given here. The DLL model fulfilled the continuity equation and provided the correlated movements of 'molecules' as in a real liquid. Moreover, the dynamic properties which it produced were in good agreement with those established for liquids [54, 55]. The simulation can be performed at the highest possible density which cannot be obtained using other models. Molecular dynamics simulations of models with a matrix of immobilized obstacles were usually performed for total concentration up to 0.6 [40, 44, 46]. This model was based on the concept of strictly cooperative motion of molecules in a dense system [54, 55]. It was based on the model of liquids where molecules vibrate near quasi-localized points (staying in a given place) and are sometimes involved in a motion correlated with neighbors resulting in a translation. This picture of a local motion in a molecular liquid was commonly accepted and documented by molecular dynamics simulations of dense hard disks and Lennard-Jones systems [62, 63]. The model was coarse-grained and beads represented entire molecules or their fragments (large obstacles were linear sequences of such beads forming polymer chains). The positions of the beads were limited to vertices of a triangular lattice and all lattice sites in the system were occupied by beads. The beads cannot move simply because all neighboring lattice sites are occupied by other objects in spite of the fact that long-range motions can be found in such systems in reality. However, the DLL model allowed the determination of the conditions required for molecular translations. Each displacement of an object from its position was considered as an attempt of a movement to a neighboring lattice site and the directions of these attempts are located along lattice vectors.

DLL cooperative rearrangements on the lattice have a form of closed loops of displacements involving at least three molecules as shown in Fig. 1. Objects that did not belong to a closed loop consisting of at least three elements were immobilized at the given time step. Immobile obstacles can be introduced in a simple way: an element belonging to an obstacle cannot take part in a cooperative loop in any case. A time unit corresponds to an attempt to change the positions of all molecules simultaneously. The simulation scheme of the DLL algorithm is the following (see Fig. 1): (1) the generation of the random vector field of motion attempts with a vector

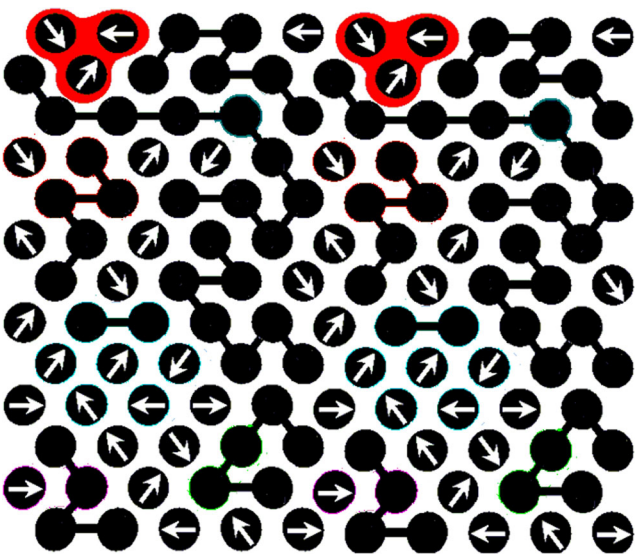

Fig. 1 The idea of the DLL model. Polymer chains are immobilized while solvent molecules can move. Effective cooperative rearrangements along closed loops are marked in red

assigned to each bead and pointed toward one of the nearest-neighboring lattice sites, (2) the selection of groups of vectors coinciding with contours of closed continuous paths (loops), showing ways of possible cooperative rearrangements, and (3) the rearrangement of objects (beads) along these closed paths (loops) by displacing them to the neighboring sites. It should be stressed that the algorithm based on the above assumptions is strictly parallel.

The single agent model (SAM) was used to compare differences in subdiffusive motion with those of the DLL model. It is equivalent to the de Gennes 'ant in the labyrinth' [26, 64, 65] and can also be treated as a variant of the Lorentz gas (in the original version of the latter model, obstacles can overlap) [4, 66]. In SAM the motion of objects takes place without any correlation with other moving objects. In the SAM model a given number of obstacles was inserted at random positions and a single agent object was placed on a randomly chosen vacant site. It then performed a random walk on vacant sites.

The simulations were performed on a triangular lattice and in the simulation box $L \times L$, where $L = 256$ with periodic boundary conditions employed along the x and y axes. It was previously shown that if the system is larger than 64×64 the statistic of cooperative loops of displacement did not depend on the size of the Monte Carlo box [54]. The trajectories usually consisted of approximately 10^8 simulation steps which is considerably more than in Brownian dynamics simulations even when a new fast algorithm was employed [38]. The simulations were repeated at least ten times and each simulation run was performed for a different matrix of randomly set obstacles (about 30 different matrices of obstacles for a given concentration of obstacles), and the results were averaged over all runs for a given set of parameters. Immobile obstacles were generated randomly as chains of beads. The concentration of obstacles was defined as the ratio of the sites occupied by the obstacles to the total number of lattice sites in the simulation box: $c = mN/L^2$, where m is the number of chains in the system and N is the length of each chain (each polymer bead has the same size as a molecule of solvent).

Results and discussion

Local topological properties of a percolating system in the critical region

There are two main factors which decide the dynamics of moving elements in crowded environments: the topology and the kind of transport. In the presented results, the topology of the system was changed by varying the length of flexible polymer chains. The scenarios of molecular transport were also varied: DLL and SAM models were used.

The mean square displacement (MSD) is a basic quantity that describes dynamics. It is defined as:

$$\left\langle \Delta r^2(t) \right\rangle = \frac{1}{n} \sum_{i=1}^{n} [\mathbf{r}_i(t) - \mathbf{r}_i(0)]^2 \quad (1)$$

where $\mathbf{r}_i(t)$ are the space coordinates of the ith molecule at time t and n is the number of considered objects (solvent molecules). The diffusion coefficient D is consequently defined by the Einstein relationship:

$$\left\langle \Delta r^2(t) \right\rangle = 4Dt \quad t \to \infty. \quad (2)$$

In disordered systems however, this law is not valid in certain conditions [26] because of the appearance of anomalous diffusion. Near the percolation threshold, the following formula can be used to describe the diffusion of objects:

$$\left\langle \Delta r^2 \right\rangle \sim t^{\alpha} \sim t^{2/d_w} \quad (3)$$

where $\alpha = 2/d_w$ is the anomalous diffusion exponent. Diffusion is hindered in these conditions, and one can find $\alpha \leq 1$ or $d_w \geq 2$ [26]. Since it is not easy to clearly see the changes of the exponent α from the course of the MSD function, we also present the MSD/time function, which makes it much easier to recognize normal (Fickian) and anomalous diffusion: the first one corresponds to a plateau (slope 0), while the latter is featured by a negative slope. These parameters, calculated for solvent molecules in systems where chains serve as immobile obstacles, are presented in Fig. 2a,b for both models of transport. The length of chains varies between $N = 8$ and $N = 256$, and their concentration is set to 0.3 in order to study macromolecular systems below ($N = 8$, 16, and 32), near ($N = 64$), and above ($N = 128$ and 256) the percolation threshold. One can observe dramatic changes of the dynamic behavior of solvent particles with an increase in polymer length for both kinds of transport. However, for the SAM model, more rapid changes are evident. For small obstacles, i.e., for short chains ($N = 8$ and 16) the diffusion of mobile objects takes place according to the Einstein formula: MSD ~ t. For longer chains ($N = 32$ and 64) one can observe that motion of solvent molecules exhibits a significant deviation from normal diffusion, i.e., a sublinear increase of MSD is visible, while for even longer chains ($N = 128$ and 256) the transition to localized motion is clearly visible. One can also observe from Fig. 2b that when increasing the chain length, and thus approaching the percolation threshold, the deviation of the exponent α from unity increases. Therefore, for chains well below this threshold ($N = 8$ and 16) the distribution of positions should be close to Gaussian. For longer chains near and above the percolation threshold, the p distribution of positions should be described by the Fox H-function. These distributions will be a subject of our further studies.

The so-called non-Gaussian parameter $\alpha_2(t)$ is a quantity that is more sensitive to changes in the character of motion than MSD. It is defined as [4, 67]:

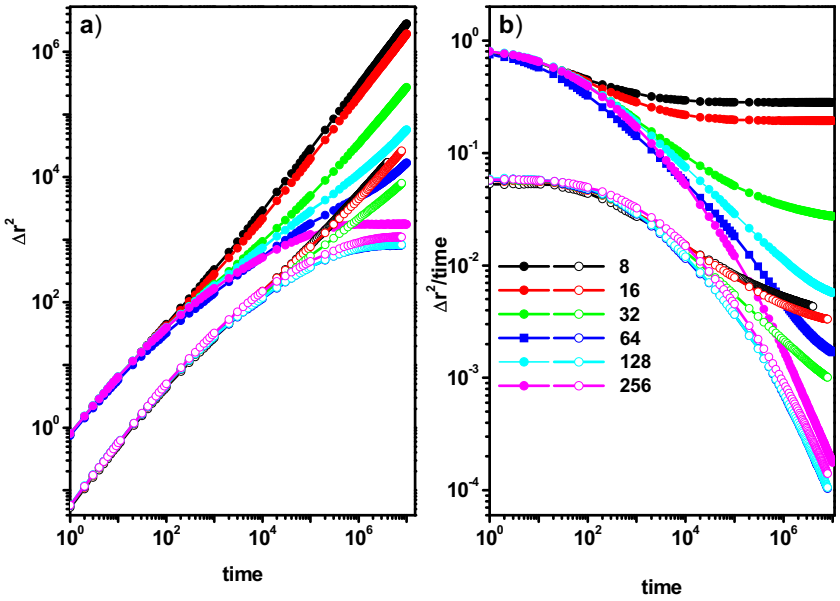

Fig. 2 MSD (**a**) and MSD/time (**b**) of solvent molecules for obstacles $N = 8$, 16, 32, 64, 128, and 256 at polymer concentration $\phi = 0.3$

$$\alpha_2(t) = \frac{\langle \Delta r^4(t) \rangle}{2\langle \Delta r^2(t) \rangle^2} - 1. \quad (4)$$

This parameter is close to zero when a normal (Fickan) diffusion takes place and exhibits a peak in the crossover to an anomalous diffusion regime. Changes of the non-Gaussian parameter with time are presented in Fig. 3a. This figure shows a clear example of changes in the dynamics of the SAM model. One can observe the transition dynamics of solvent molecules with the change in chain length: from normal diffusion through a subdiffusion behavior where one can observe a strong deviation from the Gaussian behavior to a localized motion case. In $N =$ 8, 16, and 32, the non-Gaussian parameter is close to zero as the system is far below the percolation threshold (the dependency of the percolation threshold on the chain length is given in the inset to Fig. 3) and the subdiffusive motion appears for a very short period of time. In $N = 64$, the chain system is near the percolation threshold and, therefore, the parameter $\alpha_2(t)$ rapidly increases, indicating a crossover to the subdiffusive regime. The system with chains $N = 128$ is above the percolation threshold and

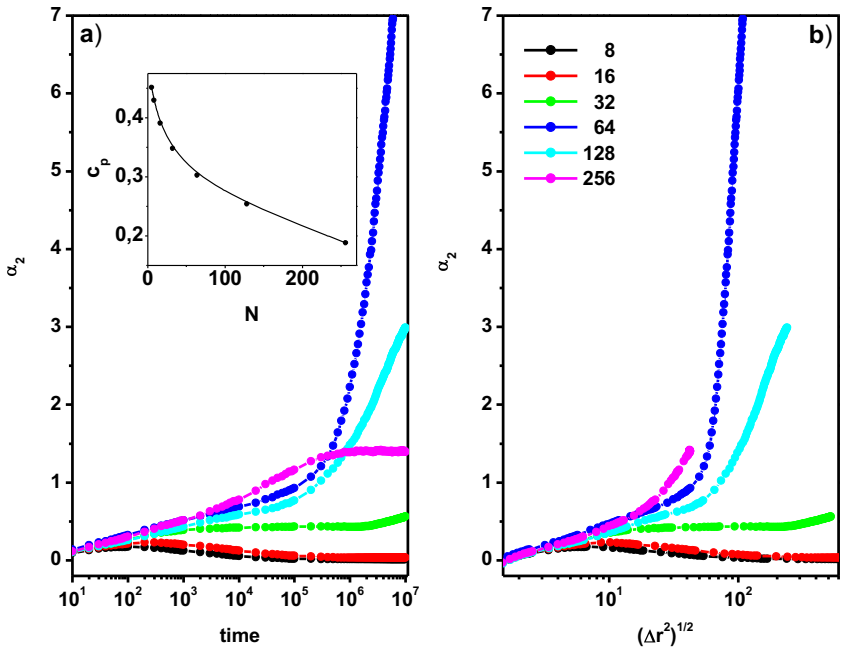

Fig. 3 Non-Gaussian parameter α_2 as a function of time (**a**) and of the displacement (**b**) for obstacles $N = 8$, 16, 32, 64, 128, and 256 at polymer concentration $\phi = 0.3$ for the SAM model. The inset presents the dependency of the percolation threshold on the chain length

hence it in the region where the subdiffusive motion begins. The system with the longest chains under consideration $N = 256$ is considerably above the percolation threshold and only localized motion can be noticed here; for this reason the $\alpha_2(t)$ plot does not display a peak. Further insight into the character of motion can be obtained by studying the changes of the parameter α_2 with the distance $(<\Delta r^2>)^{1/2}$. These plots are shown in Fig. 3b for the same polymer concentration ($\phi = 0.3$) and for various chain lengths. This type of plot is much better at showing how the diffusion changes with the mean distance traveled by molecules. The case of the chain $N = 64$ is especially interesting here: for a certain distance a rapid increase of the non-Gaussian parameter takes place. This is because of the direct proximity to the percolation threshold as confirmed by the values shown in the inset.

One can draw the conclusion that real changes of the dynamic character of solvent appear to be connected with the global topological properties of the system: the presence or the absence of a cluster formed by obstacles (polymer chains in this case) that precludes or enables the global diffusion. At this point we would like to check whether such serious changes could be connected with local properties like the geometry of an obstacle (a macromolecule) or local concentrations of solvent and polymer. In Fig. 4, we present snapshots of polymer systems at the considered concentration $\phi = 0.3$. This concentration was chosen in order to study polymer systems below, near, and above the percolation threshold. One can observe that there are no structural differences between these systems: there are chains that are completely separated one from another and deeply penetrated, and there are chains coiled as well as extended. The detailed qualitative analysis of the chains' structure will be carried out below.

The most common parameters that describe the structure of polymer chains are the following:

(i) The mean square radius of gyration $\left\langle R_g^2 \right\rangle$

$$\left\langle R_g^2 \right\rangle = \left\langle \frac{1}{N} \sum_{i=1}^{N} \left(\mathbf{r}_i - \mathbf{r}_{cm}\right)^2 \right\rangle, \tag{5}$$

where N is the total number of beads constituting the chain and $\boldsymbol{r}_{cm}$ is a coordinate of the chain's center of mass.

(ii) The mean squared end-to-end distance

$$\left\langle R_{ee}^2 \right\rangle = \left\langle \left(\mathbf{r}_1 - \mathbf{r}_N\right)^2 \right\rangle \tag{6}$$

where $\boldsymbol{r}_1$ and $\boldsymbol{r}_N$ are space coordinates of chain ends.

(iii) The gyration tensor T

$$T_{kl} = \left\langle \frac{1}{N} \sum_{i=1}^{N} \left(r_{ik} - r_{cm,k}\right)\left(r_{il} - r_{cm,l}\right) \right\rangle \tag{7}$$

where k and i are the coordinates x and y, r_{ik} is the kth coordinates of the position $\boldsymbol{r}_i$, and $r_{cm,k}$ is the kth coordinate of the chain center-of-mass. The tensor T has two eigenvalues denoted λ_1 and λ_2 (with the convention $\lambda_1 \geq \lambda_2$) called shape parameters, which fulfill the relation:

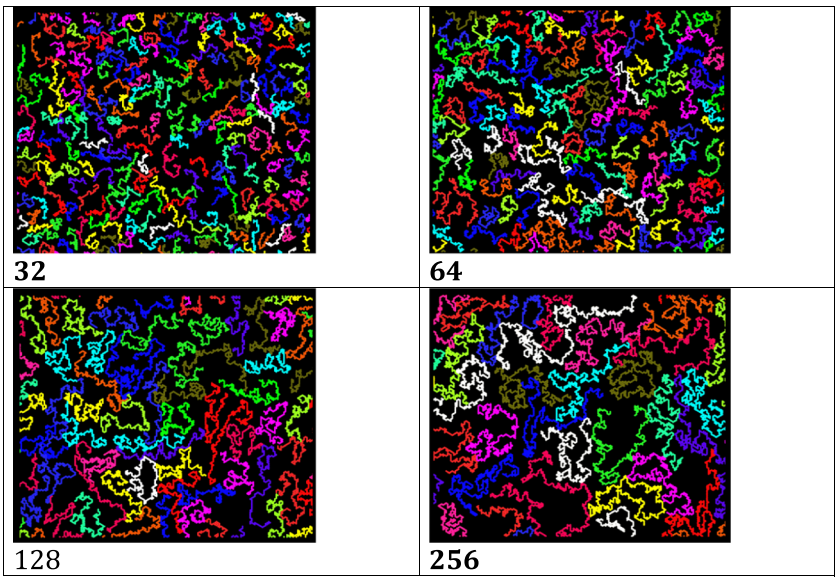

Fig. 4 Snapshots of polymer chains (obstacles) for $N = 32$, 64, 128, and 256 at polymer concentration $\phi = 0.3$

$$R_g^2 = \lambda_1 + \lambda_2 \tag{8}$$

(iv) The asphericity parameter A_2, defined as

$$A_2 = \frac{\left\langle (\lambda_2 - \lambda_1)^2 \right\rangle}{\left\langle (\lambda_2 + \lambda_1)^2 \right\rangle} \tag{9}$$

which means that that $A_2 = 1$ for a fully extended chain and $A_2 = 0$ for a disk.

(v) The intrachain site-site correlation function of sites separated by $r = \mathbf{r}_i - \mathbf{r}_j$

$$\gamma(r) = \frac{1}{n}\left\langle c(\mathbf{r}_i) \cdot c(\mathbf{r}_j) \right\rangle \tag{10}$$

where c is a contrast operator assuming values of 1 for sites occupied by molecular elements (beads) and assuming 0 everywhere else.

(vi) The intrachain static form factor:

$$S(q) = \sum_{ij} \gamma(r) \frac{\sin(qr)}{qr} \tag{11}$$

where q is the scattering vector and γ denotes the bead-to-bead correlation function defined in Eq. (10).

The parameters describing size and shape of polymer chains are shown in Fig. 5. $R_g^2, R_{ee}^2, \lambda_1, \lambda_2, A_2, R_g^2/R_{ee}^2$ are presented as functions of the chain length at the polymer concentration $\phi = 0.3$. Both size parameters R_g^2 and R_{ee}^2 are expected to scale with the chain length as:

$$\left\langle R_g^2 \right\rangle \sim \left\langle R_{ee}^2 \right\rangle \sim N^{2\nu} \tag{12}$$

This scaling behavior is generally observed, but for longer chains some deviations are clearly visible. Both shape parameters λ_1 and λ_2 exhibit a similar behavior; one can also notice that λ_1 is an order of magnitude larger than λ_2, which was expected as the shape of a chain at intermediate polymer concentration should be elongated [68]. The exponent ν, which was introduced by Flory [68], is very important in polymer physics because it shows how the size of a macromolecule scales with the chain length N (see Eq. 12), but it also describes the fractal dimension of chains d_f according to the relation $d_f = 1/\nu$. In other words, it shows how polymer chains fill the area where they are placed. Contrary to the above behavior, the remaining two parameters A_2 and R_g^2/R_{ee}^2 in Fig. 5 are almost constant, indicating that the changes in the structure of macromolecules when varying the length of chain at a given concentration are rather small. A universal scaling behavior of polymer chains at the percolation threshold was recently found [69], but despite this universality and similar structures, the dynamics of the solvent is different in the two models of transport considered.

The structural properties of polymer chains can also be analyzed using the static form factor. This parameter gives us information about the internal structure of a chain; it is also important as it can be determined in real experiments. If one considers a disk of radius r around a given bead and l beads from the same chain are present inside that disk, then $\gamma(r) \propto l/r^2$, where $\gamma(r)$ is the correlation function defined in Eq. (10). For long chains, the mean square end-to-end distance scales as $N^{2\nu}$ and, therefore, the $\gamma(r)$ function scales as $\gamma(r) \propto r^{\frac{1}{\nu}-2}$. Taking the Fourier transform and using scaling arguments one can obtain:

$$S(q) \propto q^{-\frac{1}{\nu}} \tag{13}$$

Figure 6a shows the static form factor $S(q)$ for chains $N = 32$, 64, 128, and 256 at the polymer concentration $\phi = 0.3$. In order to emphasize any deviation of the chains studied from Gaussian behavior, we additionally present Kratky plots for the same parameters, i.e., the plots of $q^2S(q)$. The slopes of linear fragments of $S(q)$ plots in Fig. 6a are the following: -1.445 ± 0.001 ($N = 32$), -1.447 ± 0.001 ($N = 64$), -1.451 ± 0.001 ($N = 128$), and -1.465 ± 0.002 ($N = 256$). The

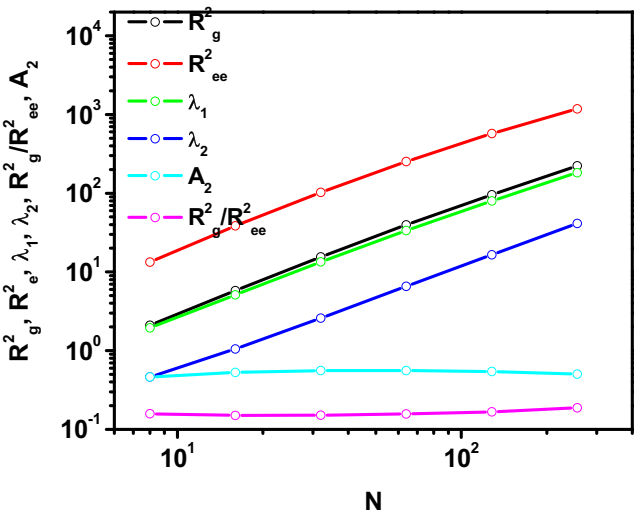

Fig. 5 The size and shape parameters of polymer chains $R_g{}^2$, $R_{ee}{}^2$, λ_1, λ_2, A_2, and R_g^2/R_{ee}^2 as functions of the chain length N at the polymer concentration $\phi = 0.3$

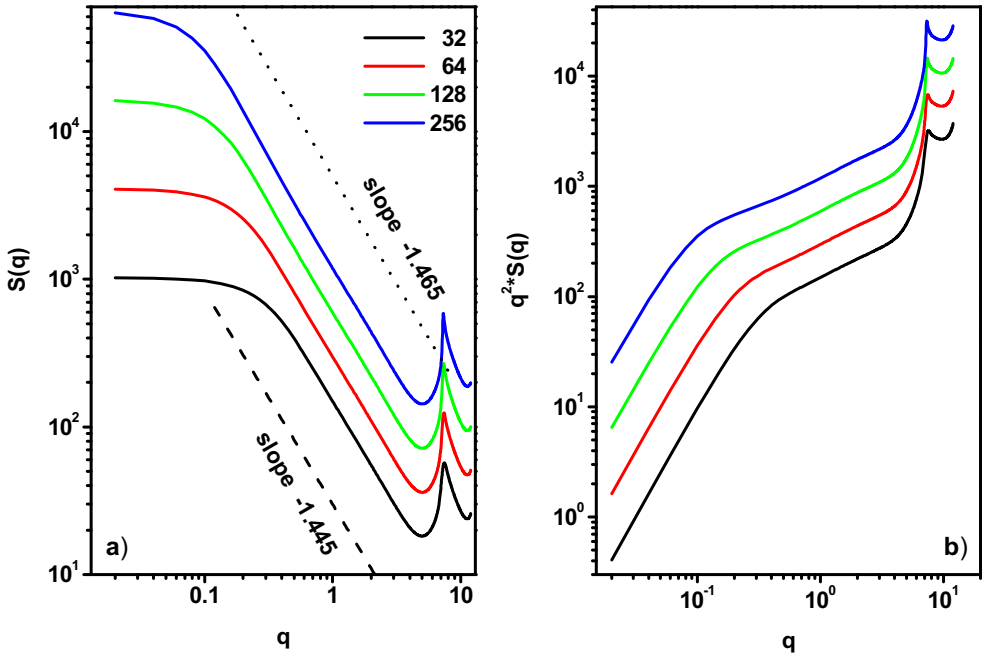

Fig. 6 Single chain form factors (**a**) and Kratky plots (**b**) for the chain length $N = 32$, 64, 128, and 256 at the polymer concentration $\phi = 0.3$. Slopes of linear fragments of plots for chains $N = 32$ and $N = 265$ are also marked in the panel a)

theoretical slope predicted for Gaussian chains in two dimensions is: −0.75 (a single chain) and −2 (at very high polymer concentrations) [68]. As the chain systems studied are at intermediate polymer concentrations, one can expect the above values in the slopes of $S(q)$ plots — the slope should correspond to $-1/\nu$. The slopes in Fig. 6a are in agreement with the values of the exponents ν calculated for the same polymer systems [70]. Similar shape of the form factor plots for different chain length confirms that the structure of chains (obstacles) does not change within the considered range of polymer length. The Kratky plot shows that there is no significant deviation form the Gaussian behavior of chains.

Dynamic behavior of the system near the percolation threshold

The dynamic behavior of moving objects near the percolation threshold is one of the main questions concerning systems containing obstacles. The dependence of the dynamics on the obstacle size and the kind of transport at the percolation point is of great importance for physical, biological, and other applications. Important and interesting dynamic characteristics of objects moving in crowded environments can be obtained from the analysis of the position autocorrelation function (PAF) defined as:

$$\rho(t) = \frac{1}{n}\sum_{i=1}^{n} m_i(0)m_i(t) \qquad (14)$$

where $m_i(0) = 1$ and $m_i(t) = 1$ or 0, depending whether or not the ith bead occupied its original position (at $t = 0$) and at a given time t, respectively. Figure 7 shows this function determined for various chain lengths near the percolation threshold for some chain lengths and employing both models of transport: DLL and SAM. One can observe that near the percolation threshold a similar behavior was found in both cases: fewer and fewer moving objects remain arrested in cages formed by immobile chains (obstacles) when the polymer length increases (caging effects correspond to plateaus observed on each curve). However, one can distinguish clear differences between the two cases: for the SAM model the decrease of PAF takes place more rapidly, which is related to the lack of correlations between moving elements in this case. The correlation between moving elements in the case of the DLL model leads to a situation where some potentially movable elements become temporary obstacles [50]; therefore, the

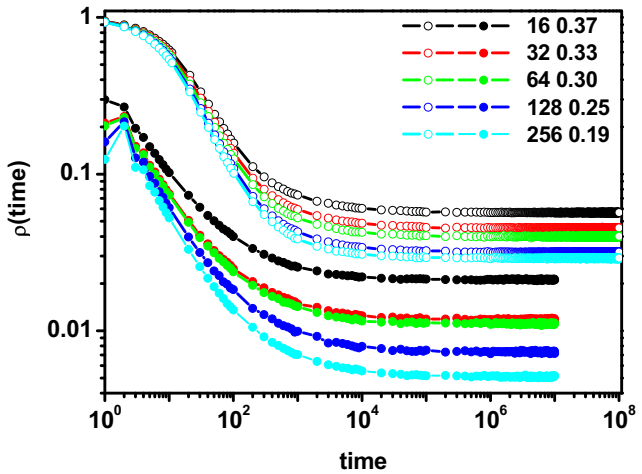

Fig. 7 The position autocorrelation function ρ(time) for various chain lengths near the percolation threshold for both models: SAM (solid symbols) and DLL (empty symbols)

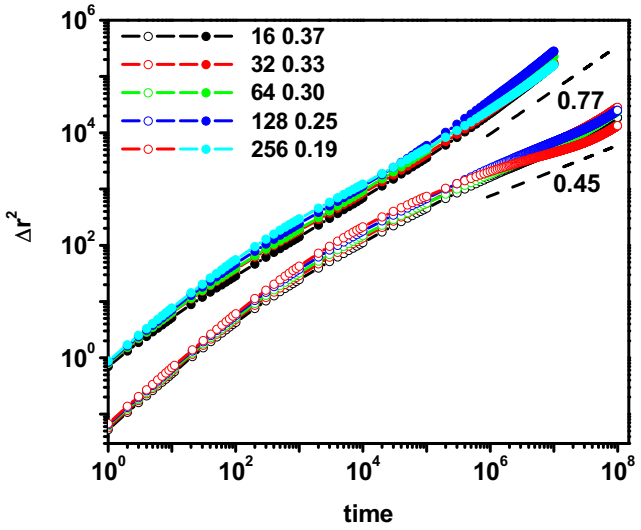

Fig. 8 MSD as a function of time near the percolation point for both models: SAM (solid symbols) and DLL (empty symbols). The chain lengths and the polymer concentrations are given in the inset

effect of trapping some of the moving elements in the case of a DLL is much stronger than in the case of SAM. It results in a weaker disappearance of the PAF function over time and a much higher plateau observed in the case of the DLL model. The heights of plateaus in plots of the PAF function depend on the chain length: the shorter the chains the higher the plateaus. This behavior is caused by differences in the polymer concentration for the systems under consideration (see inset to Fig. 3 for the changes of the percolation thresholds with chain length). In conclusion, the caging near the percolation threshold effect differs not only for models of transport but also for chains of different lengths. The influence of the caging on trajectories of moving objects is not presented here as it was already described and discussed [36, 52].

The changes of MSD with time near the percolation threshold can shed more light on the correlation between the structure of polymers (obstacles) and the dynamics of solvent molecules. Figure 8 presents MSD as a function of time for various chain lengths. For all cases under consideration in all time regimes the displacements are very similar within a given model of transport although for SAM the mobility of solvent molecules is considerably higher than for DLL. This behavior is quite different from that concerning the caging effect where the differences are significant (see the discussion above on results from Fig. 7). All MSD curves near the percolation point are quite similar despite significant differences in the size of macromolecules (obstacles) and the polymer concentration, which is rather surprising given that the structure of the polymer film was different in all cases (see Fig. 4). Slopes of the MSD curves for long time periods are approximately equal to 0.77 for the SAM model and 0.45 for the DLL model. This is more than in the case of small obstacles, where the slope was found to be 0.70 and 0.37, respectively [50, 52]. This is possibly because the distribution of small obstacles is rather uniform when compared with the structure of a polymer film (like those presented in Fig. 4). The observed similarity of the MSD behavior for systems of different sizes of obstacles near the percolation threshold and for both models of transport confirms the results obtained from the analysis of the non-Gaussian parameter α_2 as a function of time.

The direct confirmation of the above findings can be found in Figs. 9 and 10, where the non-Gaussian parameters α_2 for both models of transport (DLL and SAM) are shown near the percolation threshold. The left panels show the dependence of α_2 on time while the right panels show its dependence on the distance traveled. For both considered models only minor differences were found despite large differences between the size

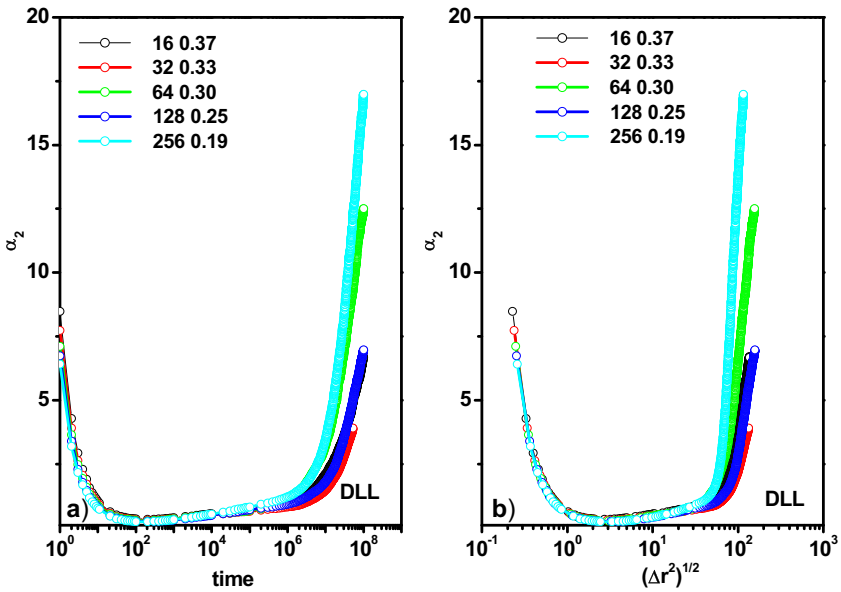

Fig. 9 Non-Gaussian parameter α_2 as a function of time (**a**) and of the displacement (**b**) near the percolation threshold for the DLL model

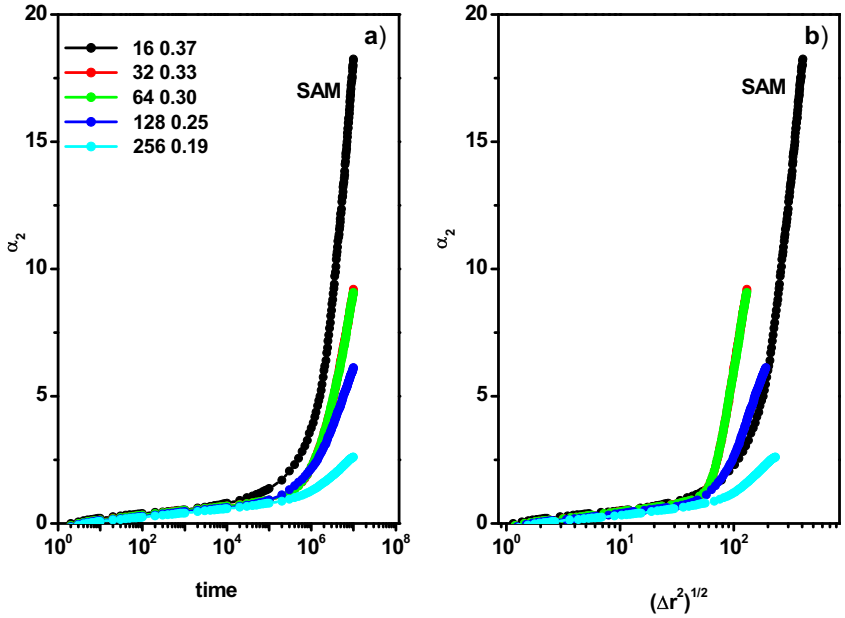

Fig. 10 Non-Gaussian parameter α_2 as a function of time (**a**) and of the displacement (**b**) near the percolation threshold for the SAM model

of obstacles and their concentration. Moreover, this similarity concerned both dependencies: time and displacement — the subdiffusive motion starts after traveling approximately the same distance in spite of differences in chain structures when changing the chain length. Large differences between α_2 values for the SAM and DLL models can be seen, which can be connected with much smaller deviation from Gaussian behavior for the SAM model than in the DLL case. The above results indicate a certain universality of the dynamic behavior within a given model of transport.

Conclusions

We used a coarse grained model for studies of the motion of probe molecules in crowded environments. The coarse-grained model was found to be suitable for studies carried out at considerably long-time scales. The model objects were beads embedded on a two-dimensional triangular lattice with excluded volume interactions only. The system was disordered by the insertion of flexible polymer chains that were immobilized and served as impenetrable obstacles. Thus, we consider a model of molecular transport in heterogeneous environment (the distribution of crowders was heterogeneous) that is characteristic for biological media. To extend our previous models [50–52] and to make them more realistic, we introduced the differentiation in size and shape of obstacles that is a typical feature of real biological systems. The main advantage of our simulation method is the possibility of studiying very dense systems where the motion of objects is strongly correlated for a very long time (seven decades). In the systems studied, the entire space was fully occupied, which was a unique feature of this method. The assessment of this simulation method was done by comparing it with a method where there were no correlations in motion of objects. The main problem addressed in this study was the microscopic mechanism of crowding-induced subdiffusion. The structure of polymer films was determined and visualized, and we focused on the question of whether there are any differences in the structure of polymer systems stemming from the fact that some of these systems hindered the motion of solvent molecules while other systems made the motion localized. To determine the dynamics of the model system, the dynamic lattice liquid algorithm was employed. It allowed for studies of dense systems (all lattice points were occupied) at considerably long time periods. In this model the motion of objects is highly correlated. A second model of molecular transport (single agent model) was also employed; a key feature of which is that there are no correlations in the motion of objects. We studied all systems at a chosen polymer concentration in order to have the system under consideration below, near, and above the percolation threshold depending on the chain length. We also investigated the systems at polymer concentration corresponding to the percolation thresholds. A normal Fickian diffusion that turned into anomalous diffusion was observed. The anomalous diffusion was transient, and the normal diffusion was recovered; however, for the polymer concentration above the percolation threshold, only localized motion was observed. The appearance of the subdiffusive behavior was shown to depend on the model of transport and the length of the macromolecules. Significant differences in mobility of movable objects appeared mainly in the subdiffusion region. The mobility of solvent molecules near the percolation threshold was found to be quite similar despite differences in the structure of chains. This holds true in spite of the universal behavior of some chain parameters. One can also conclude

that knowing the local structure of polymer film does not enable one to recognize if it is located below, near or above the percolation threshold. The above findings could be of interest when studying real biological systems, where there are differences in size and shape of moving objects. The understanding of lateral diffusion in membranes is important as this process influences other important phenomena like electron transport, receptor signaling or gating ions. A more detailed model of the motion in membranes will include interactions (binding and chemical reactions).

References

1. Ellis RJ (2001) Macromolecular crowding: obvious but underappreciated. Trends Biochem Sci 26:597–604
2. Dix JA, Verkman AS (2008) Crowding effects on diffusion in solutions and cells. Annu Rev Biophys 37:247–263
3. Zhou H-X, Rivas G, Minton AP (2008) Macromolecular crowding and confinement: biochemical, biophysical, and potential physiological consequences. Annu Rev Biophys 37:375–397
4. Höfling F, Franosch T (2013) Anomalous transport in the crowded world of biological cells. Rep Prog Phys 76:046602
5. Metzler R, Jeon J-H, Cherstvy AG, Barkai E (2014) Anomalous diffusion models and their properties: non-stationary, non-ergodicity, and ageing at the centenary of single particle tracking. Phys Chem Chem Phys 16:24128–24164
6. Montroll E, Weiss G (1965) Random walks on lattices. 2. J Math Phys (NY) 6:167–181
7. Cherry RJ, Smith PR, Morison IE, Fernandez N (1988) Mobility of cell surface receptors; a re-evaluation. FEBS Lett 430:88–91
8. Condamin S, Tejedor V, Voituriez R, Bénichou O, Klafter J (2008) Probing microscopic origins of confined subdiffusion by first-passage observables. Proc Natl Acad Sci U S A 105:5675–5680
9. Banks DS, Fradin C (2005) Anomalous diffusion of proteins due to molecular crowding. Biophys J 89:2960–2971
10. Saxton MJ (2007) A biological interpretation of transient anomalous subdiffusion. I. Qualitative model. Biophys J 92:1178–1191
11. Guglas G, Kalla C, Weiss M (2008) The degree of macromolecular crowding in the cytoplasm and nucleoplasm of mammalian cells is conserved. FEBS Lett 581:5094–5098
12. Niehaus AMS, Vlachos DG, Edwards JS, Plechac P, Tribe R (2008) Microscopic simulations of membrane molecule diffusion on corralled membrane surfaces. Biophys J 94:1551–1564
13. Fanelli D, McKane AJ (2010) Diffusion in a crowded environment. Phys Rev E 82:021113
14. Długosz M, Trylska J (2011) Diffusion in crowded biological environments: application of Brownian dynamics. BMC Biophys 4:3
15. Ramadurai S, Holt A, Krasnikov V, van den Bogaart G, Killian JA, Poolman B (2009) Lateral diffusion of membrane proteins. J Am Chem Soc 131:12650–12656
16. Szymanski J, Weiss M (2009) Elucidating the origin of anomalous diffusion in crowded fluids. Phys Rev Lett 103:038102
17. Wachsmuth M, Waldeck W, Langowski J (2000) Anomalous diffusion of fluorescent probe inside living cell nuclei investigated by spatially-resolved fluorescence correlation spectroscopy. J Mol Biol 298:677–689
18. Horton MR, Höfling F, Rädler JO, Franosch T (2010) Development of anomalous diffusion among crowding proteins. Soft Matter 6:2648–2656
19. Lindblom G, Orädd G (2009) Lipid lateral diffusion and membrane heterogenity. Biochim Biophys Acta 1788:234–244
20. Selle C, Rückerl F, Martin DS, Forstner MB, Käs JA (2004) Measurement of diffusion in Langmuir monolayers by single-particle tracking. Phys Chem Chem Phys 6:5535–5542
21. Vrljic M, Nishimura SY, Brassele S, Moerner WE, McConnell HM (2002) Translational diffusion of individual class II MHC membrane proteins in cells. Biophys J 83:2681–2692
22. Renner M, Domanov Y, Sandrin F, Izeddin I, Bassereau P, Triller A (2011) Lateral diffusion on tubular membranes; quantification of measurements bias. PLoS One 6:e25731
23. Brown FL, Leitner DM, McCammon JA, Wilson KR (2000) Lateral diffusion of membrane proteins in the presence of static and dynamical corrals: suggestions for appropriate observables. Biophys J 78:2257–2269
24. Bronstein I, Israel Y, Kepten E, Mai S, Tal-Shav Y, Barkai E, Garini Y (2009) Transient anomalous diffusion of Telomers in the nucleus of mammalian cell. Phys Rev Lett 103:018102
25. Weber SC, Spakowitz AJ, Theriot JA (2010) Bacterial chromosomal loci move subdiffusively trough a viscoelastic cytoplasm. Phys Rev Lett 104:238102
26. Ben-Avraham D, Havlin S (2000) Diffusion and reactions in fractals and disordered systems. Cambridge University Press, Cambridge
27. Sokolov IM (2012) Models of anomalous diffusion in crowded environments. Soft Matter 8:9043–9052
28. Bouchaud JP, Georges A (1990) Anomalous diffusion in random media: statistical mechanisms, models and physical applications. Phys Rep 195:127–293
29. Kammerer A, Höfling F, Franosch T (2008) Cluster-resolved dynamic scaling theory and universal corrections for transport on percolating systems. Europhys Lett 84:66002
30. Bauer T, Höfling F, Munk T, Frey E, Franosch T (2010) The localization transition of the two-dimensional Lorentz model. Eur Phys J Special Topics 189:103–118
31. Höfling F, Bamberg K-U, Franosch T (2011) Anomalous transport resolved in space and time by fluorescence correlation spectroscopy. Soft Matter 7:1358–1363
32. Sung JS, Yethiray A (2006) Lateral diffusion and percolation in membranes. Phys Rev Lett 96:228103
33. Saxton MJ (1996) Anomalous diffusion due to binding; a Monte Carlo study. Biophys J 70:1250–1262
34. Saxton MJ (2001) Anomalous subdiffusion in fluorescence Photobleaching recovery: a Monte Carlo study. Biophys J 81:2226–2240
35. Grima R, Schnell S (2006) A systematic investigation of the rate Laws valid in intracellular environments. Biophys Chem 124:1–10
36. Grima R, Yaliraki SN, Barahona M (2010) Crowded-induced anisotropic transport modulates reaction kinetics in nanoscale porous media. J Phys Chem B 114:5380–5385
37. Smith S, Cianci C, Grima R (2017) Macromolecular crowding directs the motion of small molecules inside cells. J R Soc Interface 14:20170047

38. Smith S, Grima R (2017) Fast simulation of Brownian dynamics in a crowded environment. J Chem Phys 146:024105
39. Halperin BI, Feng S, Sen PN (1985) Differences between lattice and continuum percolation transport exponents. Phys Rev Lett 54: 2391–2394
40. Sung BJ, Yethiraj A (2008) Lateral diffusion of proteins in the plasma membrane: spatial tessellation and percolation theory. J Phys Chem B 112:143–149
41. Sung BJ, Yethiraj A (2008) The effect of matrix structure on the diffusion of fluids in porous media. J Chem Phys 128:054702
42. Voigtmann T, Horbach J (2009) Double transition scenario for anomalous diffusion in glass-forming mixtures. Phys Rev Lett 103:205901
43. Kim K, Miyazaki K, Saito S (2009) Slow dynamics in random media: crossover from glass to localized motion. Europhys Lett 88:36002
44. Kurzidim J, Coslovich D, Kahl G (2009) Single-particle and collective slow dynamics of colloids in porous confinment. Phys Rev Lett 103:138303
45. Cho HW, Kwon G, Sung BJ, Yethiraj A (2012) Effect of polydispersity on diffusion in random obstacle matrices. Phys Rev Lett 109:155901
46. Skinner TOE, Schnyder SK, Aarts DGAL, Horbach J, Dullens RPA (2013) Localization dynamics of fluids in random confinement. Phys Rev Lett 111:128301
47. Kneller GR, Baczynski K, Pasenkiewicz-Gierula M (2011) Consisted picture of lateral diffusion in lipid bilayers: molecular dynamic simulation and exact results. J Chem Phys 135:3651800
48. Javanainen M, Hammaren H, Monticelli L, Jeon J-H, Miettinen MS, Martinez-Seara H, Metzler R, Vattulainen I (2013) Anomalous and Normal diffusion of proteins and lipids in crowded lipid membranes. Faraday Discuss 161:397–417
49. Goose JE, Sansom MSP (2013) Reduced lateral mobility of lipids and proteins in crowded membranes. PLoS Comput Biol 9: e1003033
50. Polanowski P, Sikorski A (2014) Simulation of diffusion in a crowded environment. Soft Matter 10:3597–3607
51. Polanowski P, Sikorski A (2016) Simulation of molecular transport in systems containing Mobile obstacles. J Phys Chem B 120:7529–7537
52. Polanowski P, Sikorski A (2017) Comparison of different models of motion in a crowded environment. A Monte Carlo study. Soft Matter 13:1693–1701
53. Polanowski P, Pakula T (2002) Studies of polymer conformation and dynamics in two dimensions using simulations based on the dynamic lattice liquid (DLL) model. J Chem Phys 117:4022–4029
54. Polanowski P, Pakula T (2003) Studies of mobility, interdiffusion, and self-diffusion in two-component mixtures using the dynamic lattice liquid model. J Chem Phys 118:11139–11146
55. Polanowski P, Pakula T (2004) Simulation of polymer–polymer interdiffusion using the dynamic lattice liquid model. J Chem Phys 120:6306–6311
56. Polanowski P, Koza Z (2006) Reaction - diffusion fronts in system with concentration dependent diffusivities. Phys Rev E 74:36103
57. Gao H, Polanowski P, Matyjaszewski K (2009) Gelation in living copolymerization of monomer and divinyl cross-linker: comparison of ATRP experiments with Monte Carlo simulations. Macromolecules 42:5929–5932
58. Polanowski P, Jeszka JK, Li W, Matyjaszewski K (2011) Effect of dilution on branching and gelation in living copolymerization of monomer and Divinyl cross-linker: modeling using dynamic lattice liquid model (DLL) and Flory–Stockmayer (FS) Model. Polymer 52:5092–5101
59. Polanowski P, Jeszka JK, Matyjaszewski K (2013) Star polymer synthesis and gelation in ATRP copolymerization: Monte Carlo simulations. Polymer 54:1979–1986
60. Lyu J, Gao Y, Zhang Z, Greiser U, Polanowski P, Jeszka JK, Matyjaszewski K, Tai H, Wang W (2018) Monte Carlo simulations of atom transfer radical (homo)polymerization of divinyl monomers: applicability of Flory-Stockmayer theory. Macromolecues 51:6673–6681
61. de Gennes PG (1979) Scaling concepts in polymer physics. Cornell University Press, Ithaca
62. Alder BJ, Wainwright TE (1959) Studies in molecular dynamics. I. General method. J Chem Phys 31:459–466
63. Barker JA, Henderson D (1976) What is "liquid"? Understanding the states of matter. Rev Mod Phys 48:587–672
64. Havlin S, Ben-Avraham S (2002) Diffusion in disordered media. Adv Phys 51:187–292
65. de Gennes PG (1976) La percolation: un concept unificateur. Le Recherche 7:919–927
66. Elizondo-Aguilera LF, Medina-Noyola M (2015) Localization and dynamic arrest of colloidal fluids in a disordered matrix of polydisperse obstacles. J Chem Phys 142:224901
67. Rahman A (1964) Correlation in the motion of atoms in liquid argon. Phys Rev 136:A405–A411
68. Teraoka I (2002) Polymer solutions. An introduction to physical properties. Wiley, New York
69. Polanowski P, Sikorski A (2018) Universal scaling behavior of polymer chains at the percolation threshold. Soft Matter 14:8249–8252
70. Żerko S, Polanowski P, Sikorski A (2012) Percolation in two-dimensional cyclic chains systems. Soft Matter 8:973–979